Ferromagnet-Insulator-Ferromagnet Tunneling with One Half-Metallic Electrode

by
Clifford T. Tanaka

B.S. Physics
Carnegie Mellon University, 1994

SUBMITTED TO THE DEPARTMENT OF MATERIALS SCIENCE & ENGINEERING IN PARTIAL FULFILLMENT OF THE REQUIREMENTS FOR THE DEGREE OF

MASTER OF SCIENCE IN MATERIALS SCIENCE & ENGINEERING
AT THE
MASSACHUSETTS INSTITUTE OF TECHNOLOGY

JUNE 1996

Signature of Author: _____
Department of Materials Science & Engineering
May 10, 1996

Certified by: _____
Ronald M. Latanision
Professor of Materials Science & Engineering

Certified by: _____
Jagadeesh S. Moodera
Research Scientist
Francis Bitter Magnet Laboratory

Accepted by: _____
Michael F. Rubner
TDK Professor of Materials Science & Engineering
Chairman, Departmental Committee on Graduate Students

Ferromagnet-Insulator-Ferromagnet Tunneling with One Half-Metallic Electrode

by

Clifford T. Tanaka

Submitted to the Department of Materials Science & Engineering on May 10, 1996 in Partial Fulfillment of the Requirements for the Degree of Master of Science in Materials Science & Engineering

ABSTRACT

Ferromagnet-Insulator-Ferromagnet (FM-I-FM) tunnel junctions were prepared with one ferromagnet being NiMnSb, a compound predicted by deGroot et al. to be half-metallic. X-ray diffraction and Rutherford back scattering experiments indicated that the deposited NiMnSb exhibited the desired structure and composition. However, a junction magnetoresistance (JMR) of only 1.5% at room temperature and 4.5% at 77K was observed for these tunnel junctions. The JMR is an order of magnitude lower than that predicted by Julliere's model of FM-I-FM tunneling, and the spin polarization was estimated to be only 8.2%. The prediction of half-metallic ferromagnetism remains unconfirmed experimentally.

Thesis Supervisor: Ronald M. Latanision
Title: Professor of Materials Science & Engineering

Thesis Supervisor: Jagadeesh S. Moodera
Title: Research Scientist, Francis Bitter Magnet Laboratory

Table of Contents

List of Figures and Tables

Acknowledgments

I would like to thank Dr. Jagadeesh Moodera for his helpful suggestions and time saving tips throughout this project. His encouragement and instruction on how to become a better scientist proved invaluable. I would also like to thank Professor Ronald M. Latanision for agreeing to serve as my faculty advisor and providing advice on my graduate career when I needed it.

Special thanks go to Dr. Janusz Nowak who worked tirelessly and unselfishly to help me with this project. His technical knowledge and creativity were essential to the progress made in this endeavor, and I have not met a more pleasant and patient person to work with.

Finally, I would like to thank my parents Herbert and Etsuko Tanaka for always encouraging me to do well in my studies. Without their support nothing I have achieved could have been possible.

1. Introduction

This thesis investigates ferromagnet-insulator-ferromagnet (FM-I-FM) tunneling in which one of the electrodes is NiMnSb, a half-metallic ferromagnet (HMF). HMFs have potentially important technological consequences because they have 100% spin polarization of their conduction electrons. Consequently, enhanced magnetic response can be observed in any spin dependent conduction phenomenon.

One of the most important characteristics of ferromagnetic materials is the splitting of the electron density of states into distinct spin up and spin down bands having different populations. The electron spin polarization (P), defined as $P = (n_\uparrow - n_\downarrow)/(n_\uparrow + n_\downarrow)$, where $n_\uparrow$ and $n_\downarrow$ are the density of states of the spin up and spin down electrons, is limited to less than 50% for conventional ferromagnets such as Ni, Co, Fe and their alloys. However, band structure calculations performed by deGroot et al. on two Heusler alloys, NiMnSb and PtMnSb predicted an entirely new phenomenon with exciting technological possibilities.[1] Analysis of the minority spin conduction electron band indicates a gap in the band structure at the Fermi level, with no corresponding gap in the majority spin band. Thus, these materials, called half-metallic ferromagnets (HMFs) by deGroot, exhibit a dual metallic/semiconducting behavior. According to this prediction, HMFs should show significantly larger conduction electron spin polarization than conventional ferromagnets, approaching 100%.

Early experiments by Meservey and Tedrow in 1973 demonstrated the phenomenon of spin polarized tunneling between a ferromagnet and a superconductor separated by an insulating barrier (FM-I-S).[2] Tunneling is a purely quantum effect in which an electron is able to pass through a potential

barrier with a given probability. In a metal-insulator-metal trilayer this tunneling probability is proportional to the density of states in one electrode at a given energy and the density of empty states at the same energy in the other electrode:

$$P(E) \sim N_1(E-eV)\, N_2(E)\, |M|^2\, f(E-eV)\, [1-f(E)],$$

where P(E) is the probability of tunneling at energy E, N_1 and N_2 are the density of states of the two metals, $|M|^2$ is the square of the matrix element describing the probability (assumed to be energy independent) and f is the Fermi function. The superconductor used by Meservey and Tedrow was aluminum, which has a number of properties which made it ideal for spin polarized tunneling experiment. First, a self-limiting aluminum oxide barrier can prepared on it, which greatly simplifies the preparation of tunnel junctions. In addition, although the bulk critical temperature (T_c) and field (H_c) are low (1.18 K and 100 gauss respectively), films sufficiently thin (~4 nm) have significantly higher T_c and orders of magnitude higher H_c . Finally and perhaps most importantly, in a magnetic field in the plane of the film, the atomic orbital response is suppressed, which means the spin response can then be observed. Consequently, in the presence of a parallel magnetic field the density of states of thin superconducting Al is split by an energy $2\mu H$, where H is the applied field, into a spin up band and a spin down band. Since a ferromagnet has different populations of spin up and spin down electrons, a conductance vs. applied voltage for a FM-I-S tunnel junction is asymmetric as shown in Figure 1.1.[3] Meservey and Tedrow exploited this effect to measure the spin polarization of various ferromagnets (Table 1.1).

These early experiments by Meservey and Tedrow strongly suggested the possibility of spin dependent tunneling between two ferromagnets

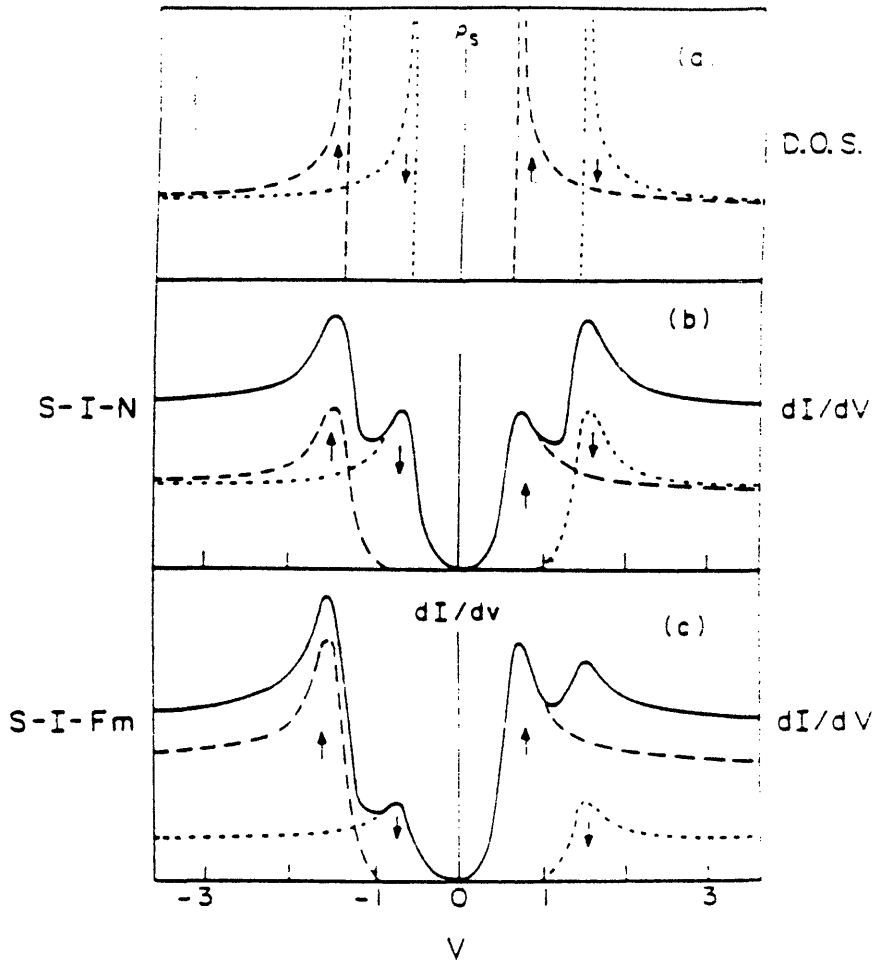

Figure 1.1 Spin Polarized Tunneling in a Magnetic Field (a) BCS density of states of a superconductor as a function of voltage. (b) conductance curve for normal metal-insulator-superconductor junction (c) conductance curve for a ferromagnet-insulator superconductor junction

Table 1.1 Spin Polarization of Tunneling Electrons for some Ferromagnets

Ferromagnet	Spin Polarization (%)
CoFe	47%
Fe	40 ± 2
Co	35 ± 3
Ni	23 ± 3
$Ni_{80}Fe_{20}$	28

(FM-I-FM), but until very recently, the change in tunneling resistance observed at room temperature was only fractions of a percent. The primary problem encountered was the difficulty in preparing a suitable artificial insulating barrier between two ferromagnets. The quality of the barrier is extremely critical because the spins of the conduction electrons must be preserved in the tunneling process or any information about the spin polarization of the ferromagnets is lost. In addition, tunneling is an extremely surface sensitive technique, involving the first one or two monolayers of the FMs. Consequently, any surface degradation of either FM would reduce the spin polarization of the tunneling electrons. Despite these difficulties, within the last two years, a change in tunneling resistance approaching 20% at room temperature has been observed in this lab by Moodera et al.[4] This breakthrough opens the door to exciting new applications for spin dependent tunneling devices including magnetic read heads and memories. A model proposed by M. Julliere predicted the change in the tunneling resistance to depend strongly on the conduction electron spin polarization of the two ferromagnets:

$$\Delta R/R_{\uparrow\downarrow} = 2 P_1 P_2/(1+P_1 P_2), \qquad (1)$$

where $R_{\uparrow\downarrow}$ is the tunneling resistance when the magnetizations of the ferromagnets are antiparallel and P_1 and P_2 are the spin polarizations of the two ferromagnets.[5] As mentioned earlier, conventional ferromagnets have spin polarizations less than 50%, which according to Eqn. (1), limits $\Delta R/R_{\uparrow\downarrow}$ to less than 40%.

The aim of this study is to take advantage of the enhanced spin polarization of a HMF by preparing FM-I-FM trilayers in which one electrode is a

HMF, NiMnSb. Even with just one HMF, thc maximum tunneling magnetoresistance should be significantly larger than that observed with two conventional ferromagnets.

2. NiMnSb: Half-Metallic Ferromagnet

NiMnSb is one of a large class of intermetallic ternary compounds known as Heusler alloys. There are two types of Heusler alloys - XYZ compounds which exhibit $C1_b$ structure and X_2YZ compounds which exhibit $L2_1$ structure. These alloys form a crystal structure consisting of four interpenetrating FCC sub-lattices A,B,C and D with coordinates: A (0,0,0); B (1/4,1/4,1/4); C (1/2,1/2,1/2); and D (3/4,3/4,3/4) as shown in Figure 2.1a. In the $L2_1$ structure, sites A and C are occupied by a transition or noble metal atom X while in the $C1_b$ structure A is occupied and C is unoccupied. Site D is occupied in both structures by a Z atom, which is a group III, IV or V B element. Figure 2.1b shows the crystal structure of the $C1_b$ NiMnSb compound.[6]

A great deal of work has been done in the past on Mn based Heusler alloys, i.e. XMnZ and X_2MnZ, by Persson[7,8] and Bradley and Rodgers[9] which pointed to the importance of the Mn sites in the ferromagnetic character of these alloys. Persson found that ferromagnetism occurred in the $(CuMn)_3Al$ series only when the Mn concentration was at least 19 at.%. Bradley and Rodgers later found that $Cu_{2.2}Mn_{0.65}Al_{1.15}$ annealed at 500 °C and slowly cooled resulted in a nonmagnetic phase. Quenching the same compound from 800°C resulted in a ferromagnetic phase with a fcc Mn sub-lattice. Later work by Webster (1969) employing neutron diffraction showed that the magnetic moment in most Mn based Heusler alloys was confined to the Mn sites and was approximately 4 Bohr magnetons. Thus, the atomic ordering of Mn sites is critical in determining the magnetic properties of these Heusler alloys.

DeGroot et al's calculation predicting HMF behavior in NiMnSb[1] (and also PtMnSb, another Heusler alloy) used the augmented-spherical-wave-

a)

b)

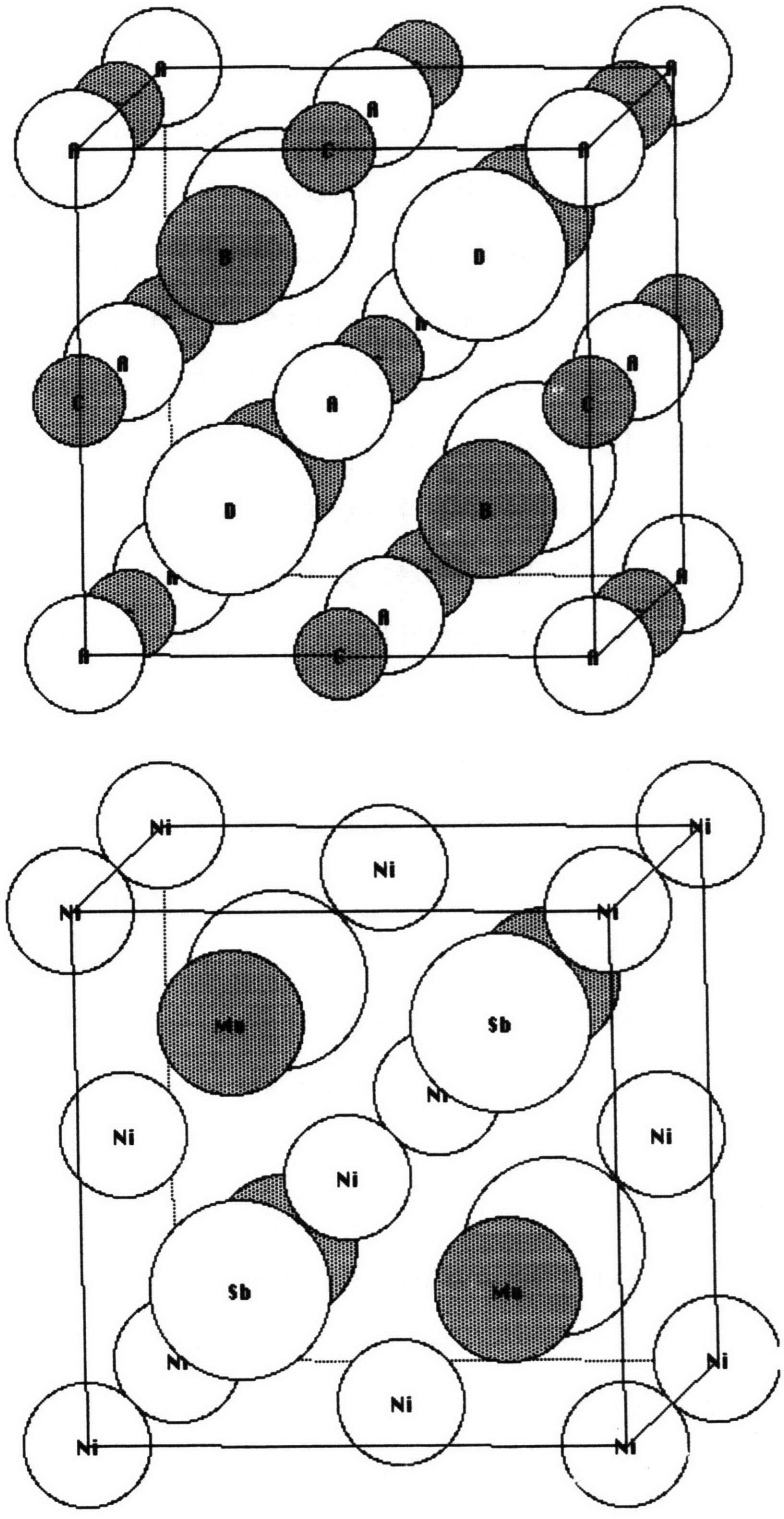

Figure 2.1 a) $L2_1$ crystal structure of Heusler alloys
b) $C1_b$ crystal structure of NiMnSb (site C is empty)

developed by Methfessel and Kubler.[11] Spin-orbit interactions were not included however, which would tend to shrink the bandgap. The existence of the bandgap was attributed to the reduction in point symmetry of the Mn sites from O_h in the $L2_1$ structure to T_d in the $C1_b$ structure. This loss of inversion symmetry breaks the conjugation or spin flip symmetry. The resulting change in the Sb p electron interactions with the Mn t_{2g} electrons results in the Sb p levels pushed above the Fermi level in the majority band case while still connected with lower states. This results in metallic behavior in the majority band. In the minority band case the Sb p levels are pushed below the Fermi level, thus opening an energy gap. Figure 2.2 shows the band structure calculated by deGroot et al. In the case of NiMnSb, the predicted energy gap is approximately 0.5 eV, which is large enough that the gap will persist even if the spin-orbit interactions are included.

Experimental evidence for HMF behavior has been largely inconclusive. Recent related work by R. Kabani at this laboratory was unable to confirm deGroot's prediction using spin polarized tunneling between NiMnSb and an Al superconducting layer as Meservey and Tedrow had done in their studies of other ferromagnets.[12] The primary problem encountered by Kabani was the inability to resolve the Zeeman splitting of the Al superconducting layer in a magnetic field as shown in Figure 2.3. This was largely attributed to the surface roughness of the NiMnSb film. Since the constraints of NiMnSb preparation required that the NiMnSb be deposited first, any surface roughness of the NiMnSb layer would affect the morphology of the upper Al layer. Consequently, the Al layer was not smooth and uniform enough to observe the Zeeman splitting of the superconducting state. Any magnetic field applied would not be

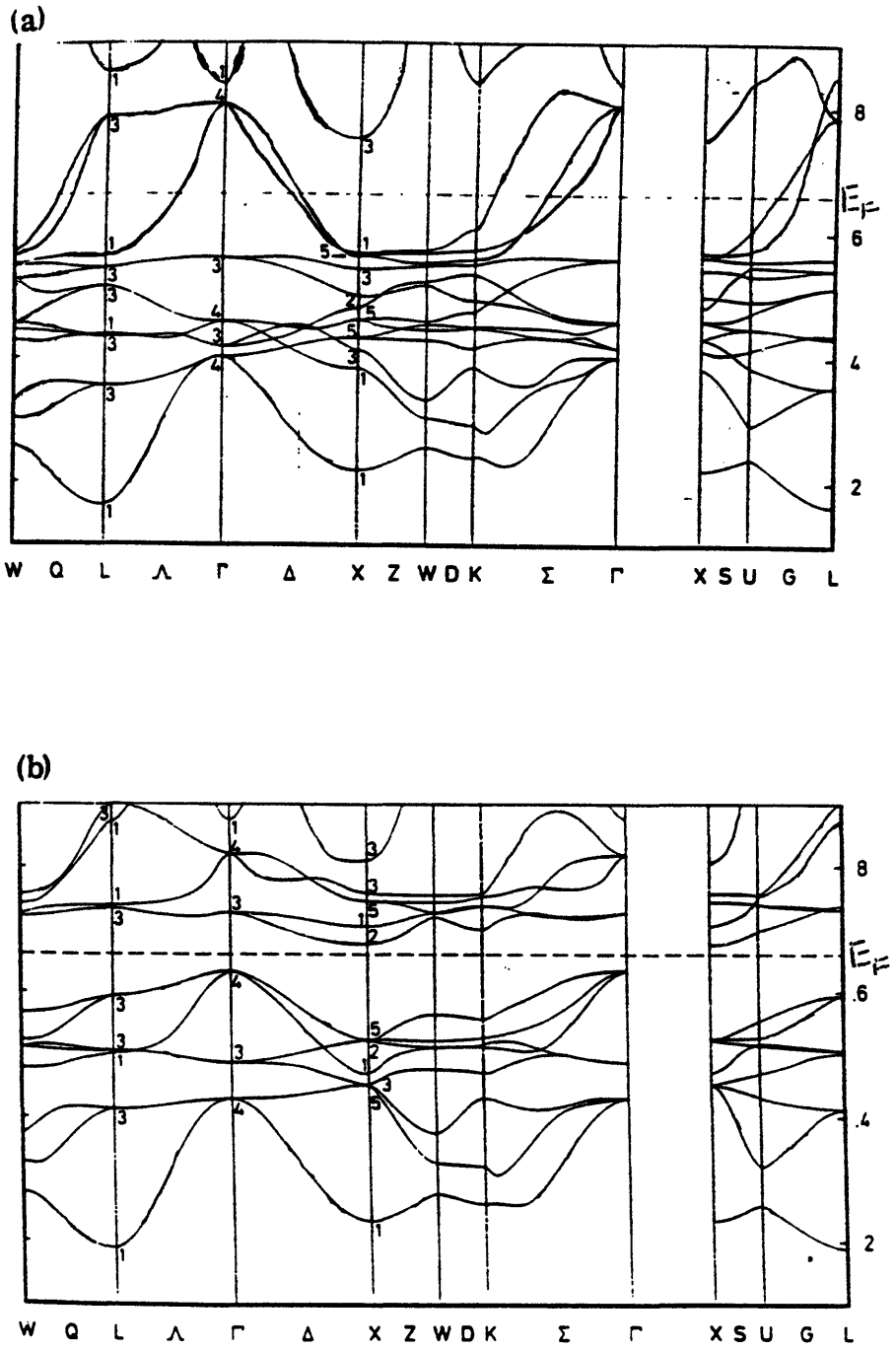

Figure 2.2 Band Structure of NiMnSb as calculated by deGroot, et al. a) Majority spin band b) Minority spin band

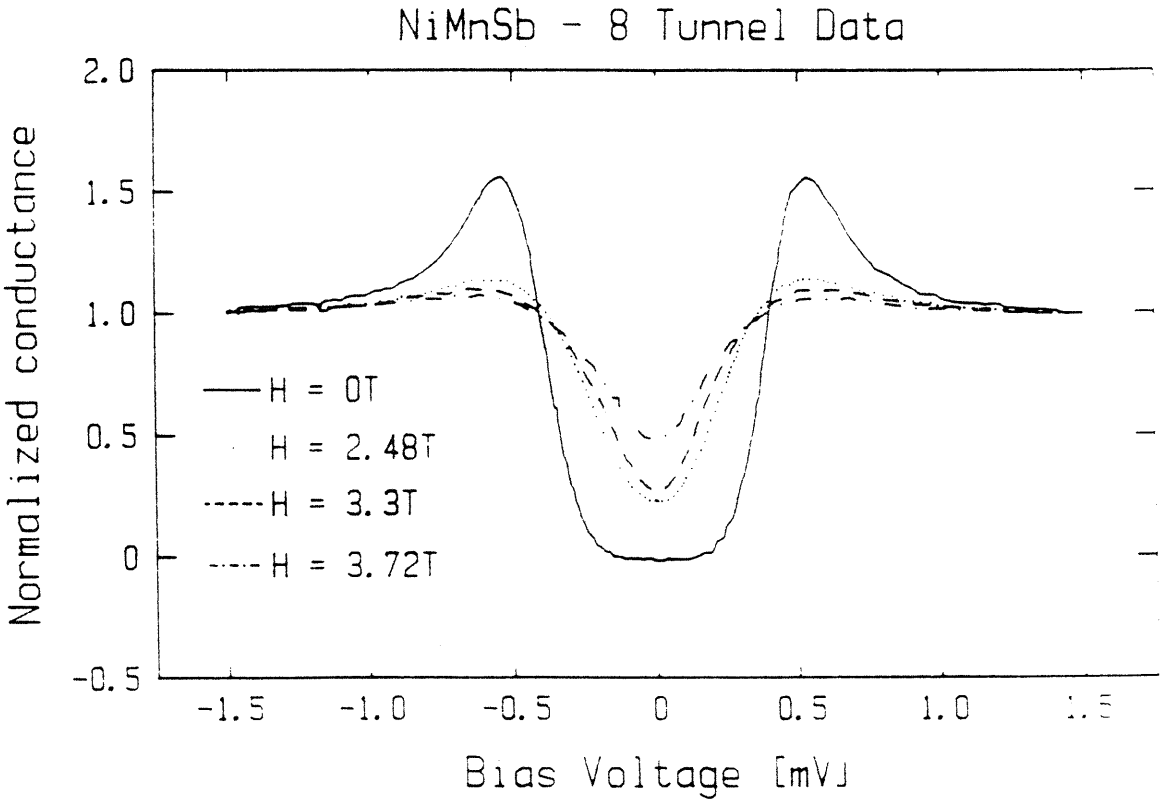

Figure 2.3 Tunnel conductance curves for NiMnSb/Al_2O_3/Al junction measured by Kabani. Note the lack of Zeeman splitting.

strictly in the plane of the film, resulting in orbital depairing which obscures the Zeeman splitting of the Al superconductor into two spin states. This prevented Kabani from measuring the spin polarization of NiMnSb.

Other measurements of the transport properties of NiMnSb and PtMnSb films performed by Moodera and Mootoo were consistent with the prediction of HMF in these materials.[13] For example, they discovered that the temperature dependence of the resistivity (ρ) showed unusual behavior. In normal ferromagnets such as Ni and Fe, spin flip scattering due to magnons results in a T^2 dependence of ρ below 20K[14], whereas HMF compounds indicated a linear relationship between ρ and T as shown in Figure 2.4. Recall that in a HMF, the spin down density of states is empty at the Fermi energy, so the spin flip of charge carriers is forbidden. Thus, the absence of T^2 dependence for ρ is consistent with HMF in NiMnSb and PtMnSb. In addition, the ordinary Hall coefficient (R_o) for NiMnSb showed a factor of seven increase from 295K to 4.2K (see Figure 2.5) which indicates a decrease in the carrier density at low temperature, again in agreement with the prediction of a bandgap in the minority spin band. However, although these observations show consistency with HMF, they are by no means proof of it.

Other experiments were also performed to measure the spin polarization of NiMnSb. Spin polarized photoemission experiments by Bona et al. measured a spin polarization of only 50%.[15] However, the limitations of this surface sensitive technique, such as surface segregation of one of the elements, damage of the first layer of NiMnSb due to the presence of the surface and surface magnetic effects could diminish the spin polarization measured. In addition, this technique is unable to sample very near the Fermi energy because of the extremely small signal near E_f. Nevertheless, Bona

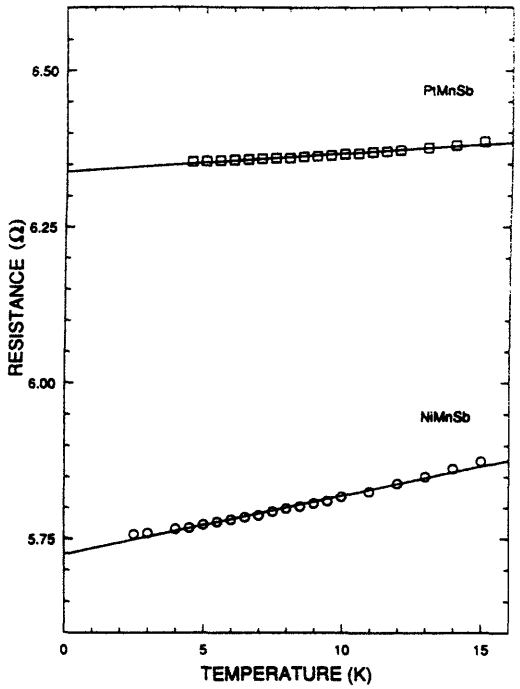

Figure 2.4 Resistivity vs. T for NiMnSb film at low temperatures (Moodera and Mootoo, 1994)

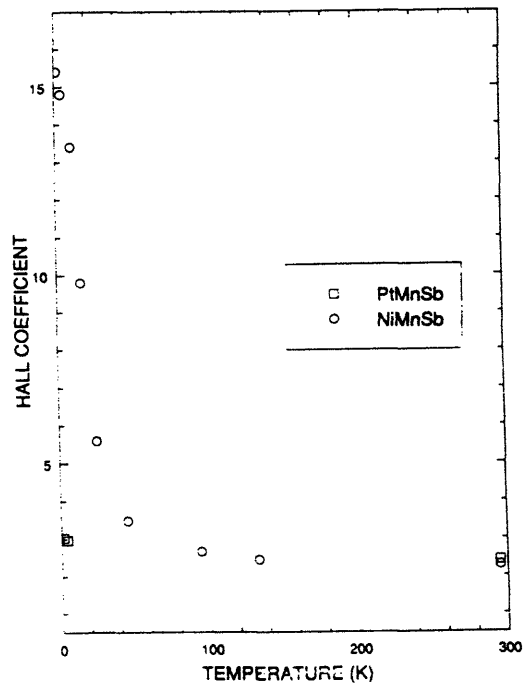

Figure 2.5 Ordinary Hall coefficient as a function of temperature from 300K to 4.2K (Moodera and Mootoo, 1994)

concluded that the energy gap of NiMnSb must be less than 0.5 eV. This conclusion was also proposed by Rau et al., who measured a polarization of only 13% using electron capture spectroscopy.[16] A recent study by Kirrilova et al. measured the interband optical absorption to estimate the energy gap of NiMnSb at 0.4 eV.[17] As mentioned earlier, a possible reason for the reduced E_g suggested by these experiments was the exclusion of spin-orbit interactions in deGroot's calculation.

3. Model of Ferromagnet-Insulator-Ferromagnet Tunneling

In 1975, Julliere extended the concept of spin polarized tunneling to tunneling between ferromagnets and proposed a simple model which assumes that spin polarization is conserved in the tunneling process and that the tunneling probability depends on the density of states of the two ferromagnets. As a result, the tunneling probability depends on the relative orientation of the FMs. This model predicts a change in tunneling magnetoresistance of:

$$\Delta R/R_{\uparrow\downarrow} = 2 P_1 P_2/(1+P_1 P_2),$$

where $R_{\uparrow\downarrow}$ is the tunneling resistance when the magnetizations of the ferromagnets are antiparallel and P_1 and P_2 are the spin polarizations of the two ferromagnets. In practice, a magnetic field dependent device can be realized by engineering the FM electrodes to have different coercivities. From the saturated parallel state, the antiparallel orientation can be achieved in the field region between the two coercivities, where the softer FM will have reversed magnetization while the harder FM will not. Julliere measured a conductance change of 14% at 4.2K in a Fe/Ge/Co tunnel junction. However, this effect appeared to be a zero bias anomaly possibly resulting from interactions with localized moments. At biases of a few millivolts, the effect dropped to less than 1%.

Many later groups investigated FM-I-FM with limited success. Junction magnetoresistances of only a few percent at 4.2K was observed, which dropped to a few tenths of a percent at room temperature. Then in 1994, Moodera et al. achieved a tunnel junction magnetoresistance (JMR) of 11.8% in

CoFe/Al_2O_3/Co or NiFe junctions at room temperature, much higher than previous results.[4] The effect increased with decreasing temperature, to 20% at 77K and 24% at 4.2K. Further refinements achieved a maximum of 18% at room temperature and 25.6% at 4.2K. Figure 3.1 shows the tunnel magnetoresistance of a CoFe/Al_2O_3/NiFe junction exhibiting high magnetoresistance at room temperature. Another group in Japan reported a similar breakthrough with Fe/Al-Al_2O_3/Fe junctions showing 18% at room temperature.[18]

The significance of half-metallic ferromagnets is now clear. With one 100% polarized electrode, Julliere's model predicts that a JMR of 50% or more is possible (e.g. for Fe with P=40% a JMR of 57% is predicted for HMF/Al_2O_3/Fe), a marked increase over current results with conventional ferromagnets. Technologically, the advantage of this enhanced JMR is obvious. Scientifically, observing this enhanced JMR will be strong evidence supporting deGroot's prediction of half metallic ferromagnetism. It should be noted that this study, by using a ferromagnet electrode opposite the HMF, avoids completely the problem of the absence of Zeeman splitting in an orbitally depaired superconductor encountered by Kabani.

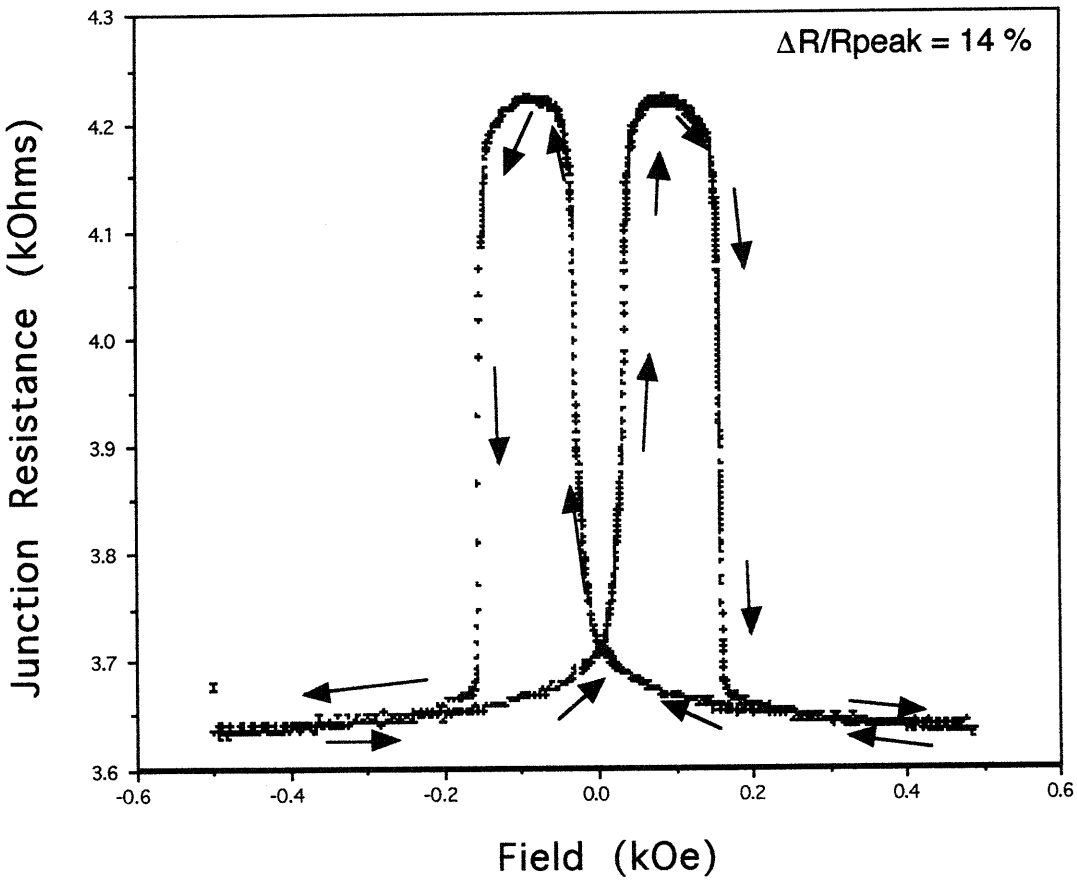

Figure 3.1 Measurement of FM-I-FM tunnel junction exhibiting high JMR at room temperature (Moodera, et al. 1995).

4. Preparation and Characterization of NiMnSb Films

4-1. Preparation of NiMnSb Thin Films

Bulk polycrystalline NiMnSb has been prepared in the past by melting the three elements at 1000°C-1200°C under low argon pressure in sealed quartz capsules and subsequently annealing for 1-15 days in vacuum or nitrogen atmosphere.[18] The samples are then quenched to freeze in the $C1_b$ NiMnSb phase. Kabani investigated the properties of NiMnSb thin films prepared under high vacuum (~10^{-7} Torr) with different deposition and annealing temperatures. The films were deposited on heated glass substrates by co-evaporating each of the three elements Ni, Mn and Sb simultaneously. A minimum annealing temperature of about 300°C was required to observe the desired $C1_b$ NiMnSb phase as determined by x-ray diffraction measurements, while annealing above 650°C seemed to destroy this phase. It was also discovered that higher deposition temperatures reduced the required annealing times drastically. The optimum temperature to reduce the anneal time to only a few minutes was found to be about 500°C. After annealing, the films were cooled rapidly with liquid N_2.

The preparation of NiMnSb thin films in this study largely followed the recipe outlined by Kabani in her 1992 Ph.D. thesis, although the annealing step was eliminated in most junctions prepared. This was done to minimize the surface degradation of the NiMnSb which could occur more readily at elevated temperatures. The films were prepared in a NRC-3116 high vacuum evaporator which achieved base pressures of about 5 X 10^{-8} Torr with the help of a liquid nitrogen cooled Meissner trap above the substrate. A schematic of the interior

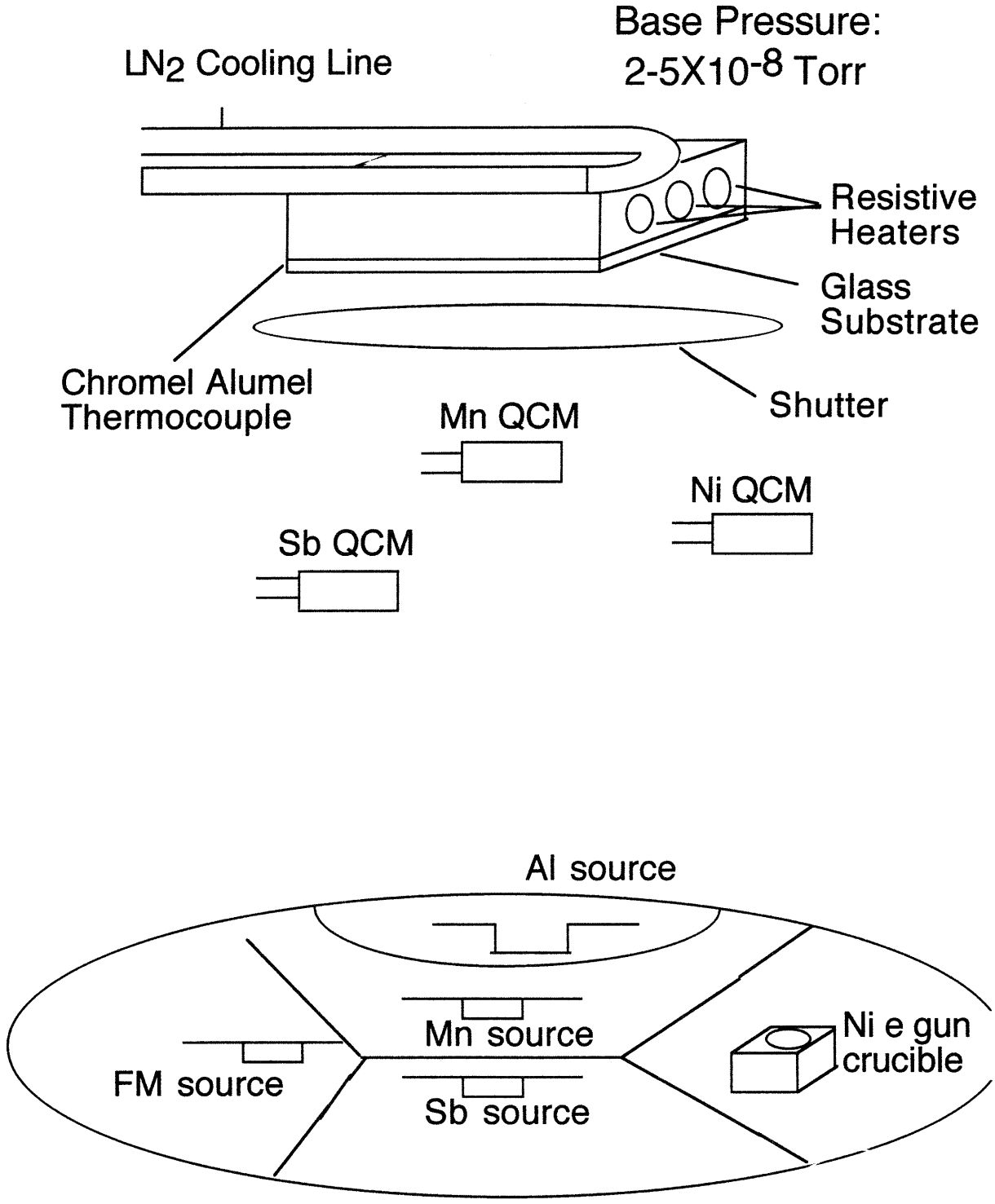

Figure 4.1 Schematic of Evaporation System

of the system is shown in Figure 4.1. Ni was evaporated from a copper crucible with an electron beam gun, while Mn and Sb were evaporated from molybdenum and tantalum boats respectively. Each source was monitored by a separate quartz crystal monitor, so the stoichiometry of the film could be fairly well controlled, to within about 1-2%. The substrates were mounted on a copper block which could be heated using three resistive heaters as well as cooled using the attached cooling lines. A thermocouple was attached near the substrates to monitor the temperature of the block.

Substrates used in most instances were precleaned glass slides, although a few trials were performed on silicon wafers and mica. Later substrates were covered with a thin (~15 Å thick) Al layer, which was then oxidized by glow discharge to form an Al_2O_3 layer before the deposition of NiMnSb. This Al_2O_3 layer significantly improved the adhesion of the NiMnSb to the substrate. The temperature during NiMnSb deposition was varied from 300-500°C. The rate of deposition used was usually 1.0 Å/sec. After NiMnSb deposition, the substrate was quenched with liquid N_2.

4-2. X-ray Diffraction

X-ray diffraction was performed on several NiMnSb samples prepared at different temperatures to determine if they exhibited the correct $C1_b$ crystal structure. A Rigaku 200 diffractometer with thin film attachment was used with an incident angle (theta) fixed at 1.5°. A voltage of 50 kV and current of 40 mA were used, and the scan was performed over a 2 theta range of 25°-85°. The diffraction patterns for the samples analyzed is shown in Figures 4.2, 4.3 and 4.4.

The diffraction patterns indicate that all of the samples show the

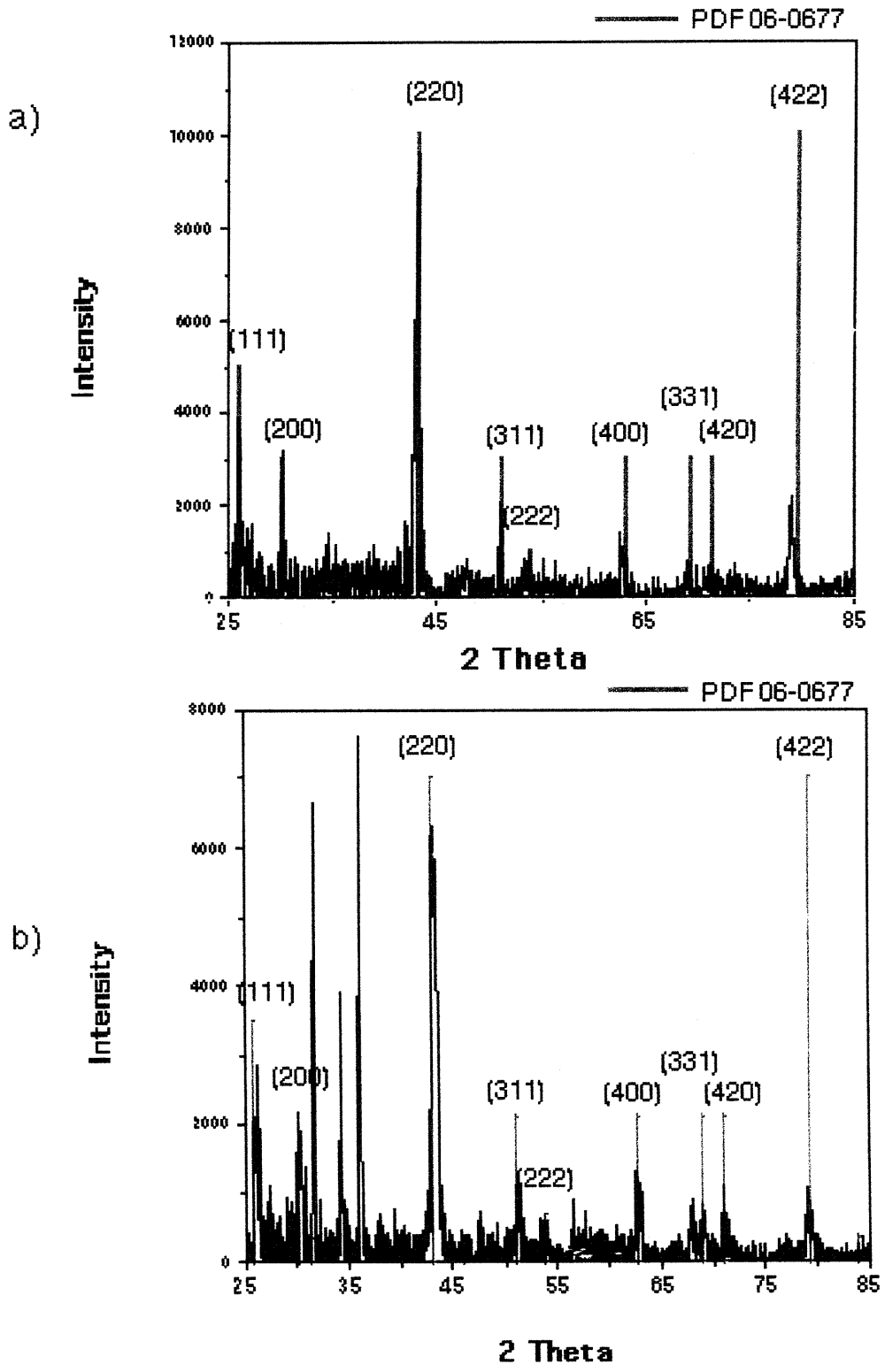

Figure 4.2 X-ray Diffraction Patterns:
a) series 10-283 300 Å NiMnSb grown on glass at 450°C
b) series 10-284 300 Å NiMnSb grown on Si wafer at 300°C

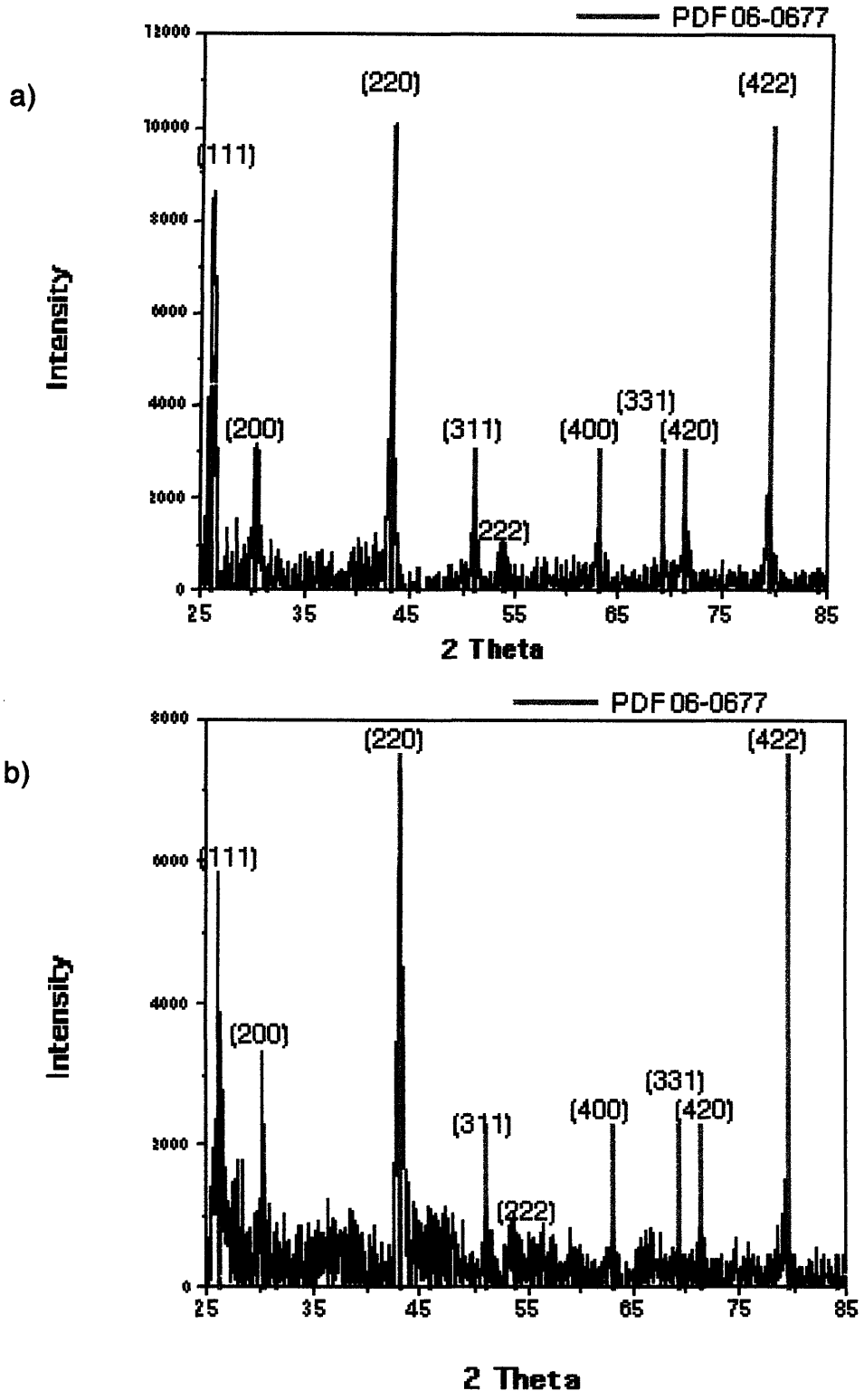

Figure 4.3 X-ray Diffraction Patterns

a) series 10-285 300 Å NiMnSb grown on glass at 400°C
b) series 10-286 300 Å NiMnSb grown on glass at 450°C

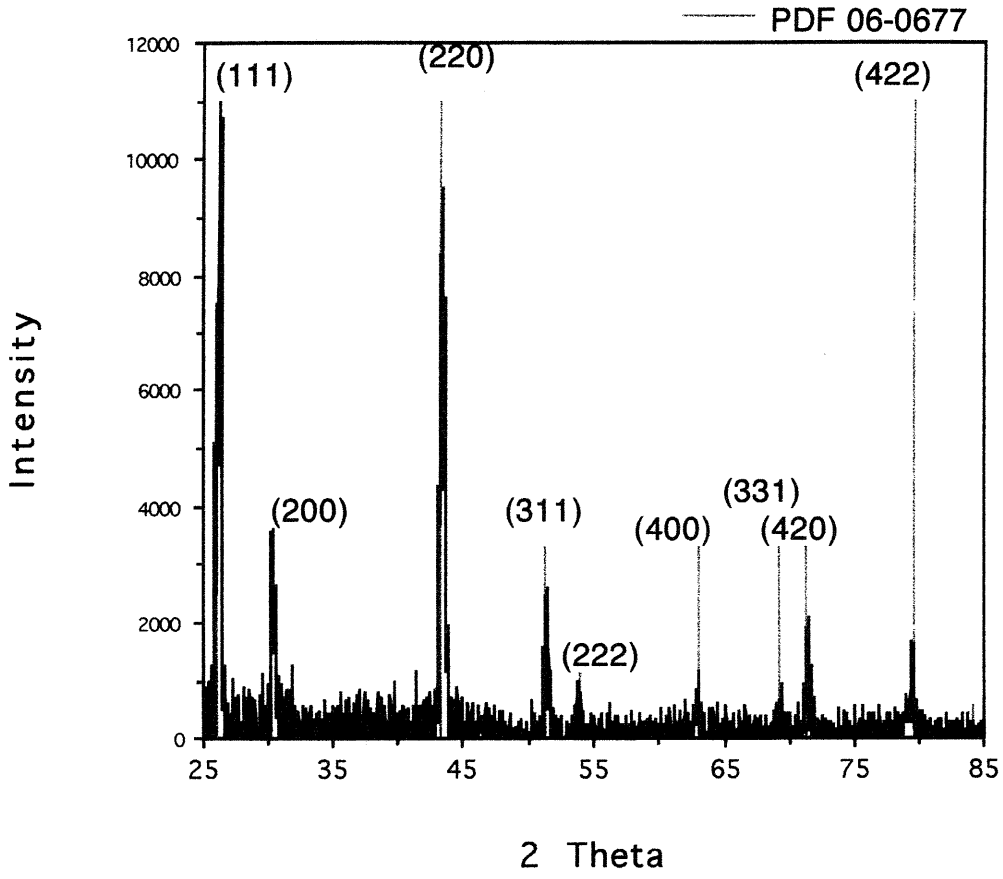

Figure 4.4 X-ray Diffraction Pattern:
Series 10-288 750Å NiMnSb on glass at 500°C.

Table 4.1

Series	Lattice Parameter
10-283	5.918 Å ± 0.025 Å
10-284	5.913 Å ± 0.017 Å
10-285	5.902 Å ± 0.010 Å
10-286	5.894 Å ± 0.010 Å
10-288	5.897 Å ± 0.010 Å
Average	5.905 Å ± 0.009 Å
PDF 06-0677	5.903 Å

characteristic $C1_b$ structure. In all cases the peak positions are in good agreement with the polycrystalline NiMnSb powder diffraction file (PDF) data. Lattice parameters were calculated for each of these samples and are shown in Table 4.1. All of the lattice parameters agreed with the PDF value of 5.903 Å. In addition, no evidence of any additional undesired phases was observed on any of the samples deposited on glass. The additional peaks in the sample deposited on Si are due to the Si substrate. Examination of the peak heights of the diffraction patterns reveals a marked difference between the relative heights of the (111) peaks of the samples. The (111) peaks in Figures 4.3a,b and 4.4 are much more prominent than in polycrystalline NiMnSb. This indicates growth in a preferred (111) orientation. In contrast, the samples in Figure 4.2 do not show this preferred orientation

4-3. Rutherford Back Scattering

Rutherford back scattering (RBS) experiments were performed in order to confirm the NiMnSb composition was in the correct 1:1:1 ratio. RBS involves the bombardment of a sample with positively charged He nuclei. The particles are scattered due to the Coulomb interaction of the ions with the nuclei within the sample. The total scattering cross section depends on the square of the charge of the target nuclei while the energy of the scattered particles depends on the mass of the target nuclei. The latter fact allows the scattering cross section to be resolved separately by element. Relative abundances of elements in a sample can thus be determined by measuring the RBS cross section due to

a given element and dividing by the square of the element's atomic number.

A sample of NiMnSb 150 Å thick was prepared on a silicon wafer for RBS analysis. The ratio of the elements deposited as determined by the quartz crystal thickness monitors was 0.98:0.95:1.00. A standard sample consisting of a thin layer of gold on silicon was first analyzed to provide a standard for comparison. The incident beam consisted of alpha particles with an energy of 3.0 MeV. Several samples were analyzed from the same wafer. Figure 4.5a-b and Figure 4.6a show the energy spectra from these measurements. The positions of the Mn and Sb peaks agreed well with the expected positions determined from the gold peak and the Si edge from the standard sample. However, the Ni peak was shifted slightly and also broadened somewhat. This could be due to diffusion of Ni into the silicon. Each of the three peaks was integrated and divided by the square of the atomic number of the corresponding element. The average ratio of the three elements Ni, Mn and Sb respectively was found to be 1.03: 0.94: 1.00 with a precision of about 5%. Note that the overlap of the Ni and Mn peaks results in some uncertainty in the first two numbers. To better resolve the Ni and Mn peaks, a scan with 4.5 MeV alpha particles was performed. Figure 4.6b indicates that much better resolution is achieved for the Ni and Mn peaks at this higher energy. The ratio determined from this data was 1.03: 0.96: 1.00. The RBS data is in good agreement with the ratio determined by the thickness monitors. The control of the ratio (as determined by the thickness monitors) for other trials was usually much better, to within 2%.

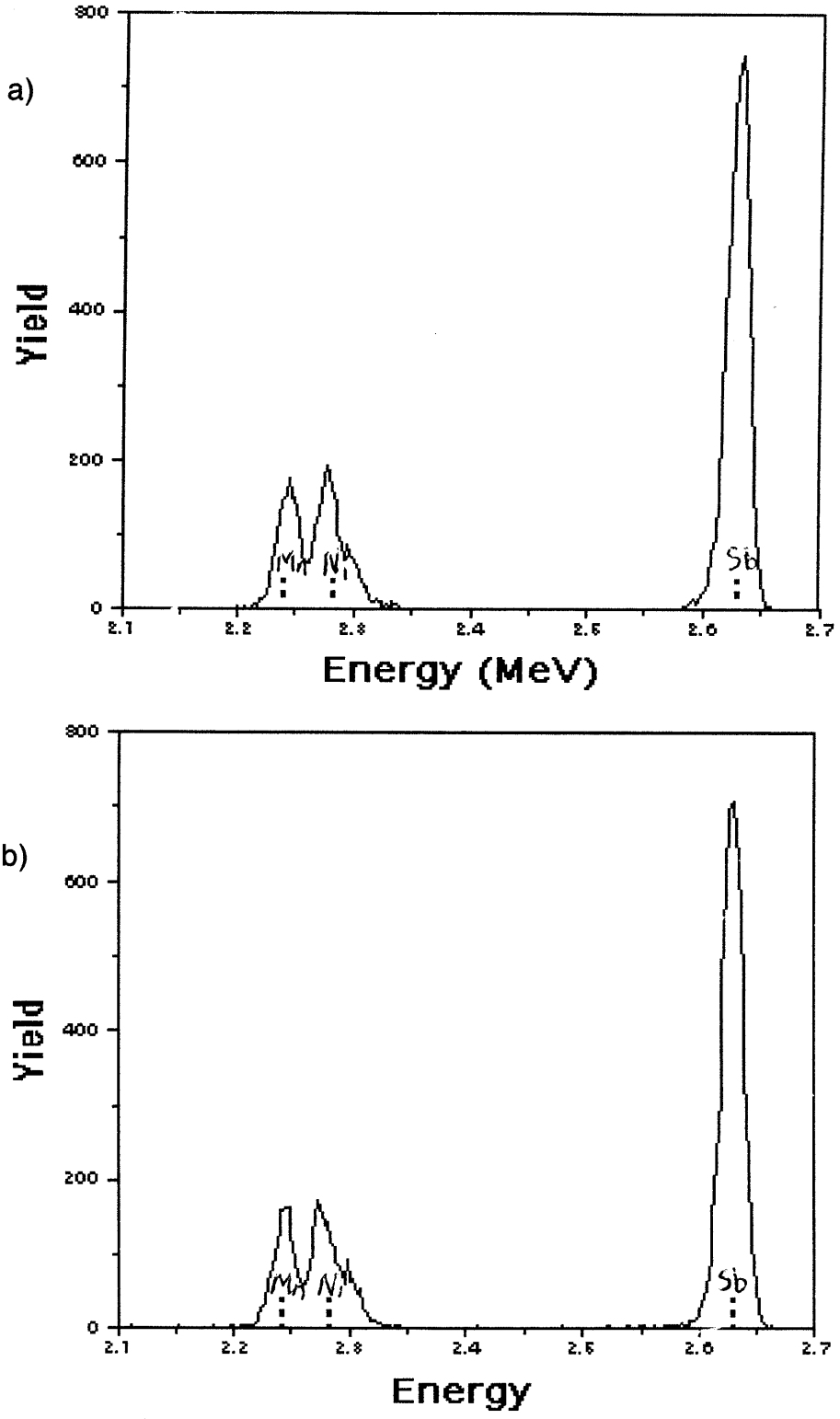

Figure 4.5 RBS Spectra for 150 Å NiMnSb on Si
a) sample 1 at 3.0 MeV b) sample 2 at 3.0 MeV

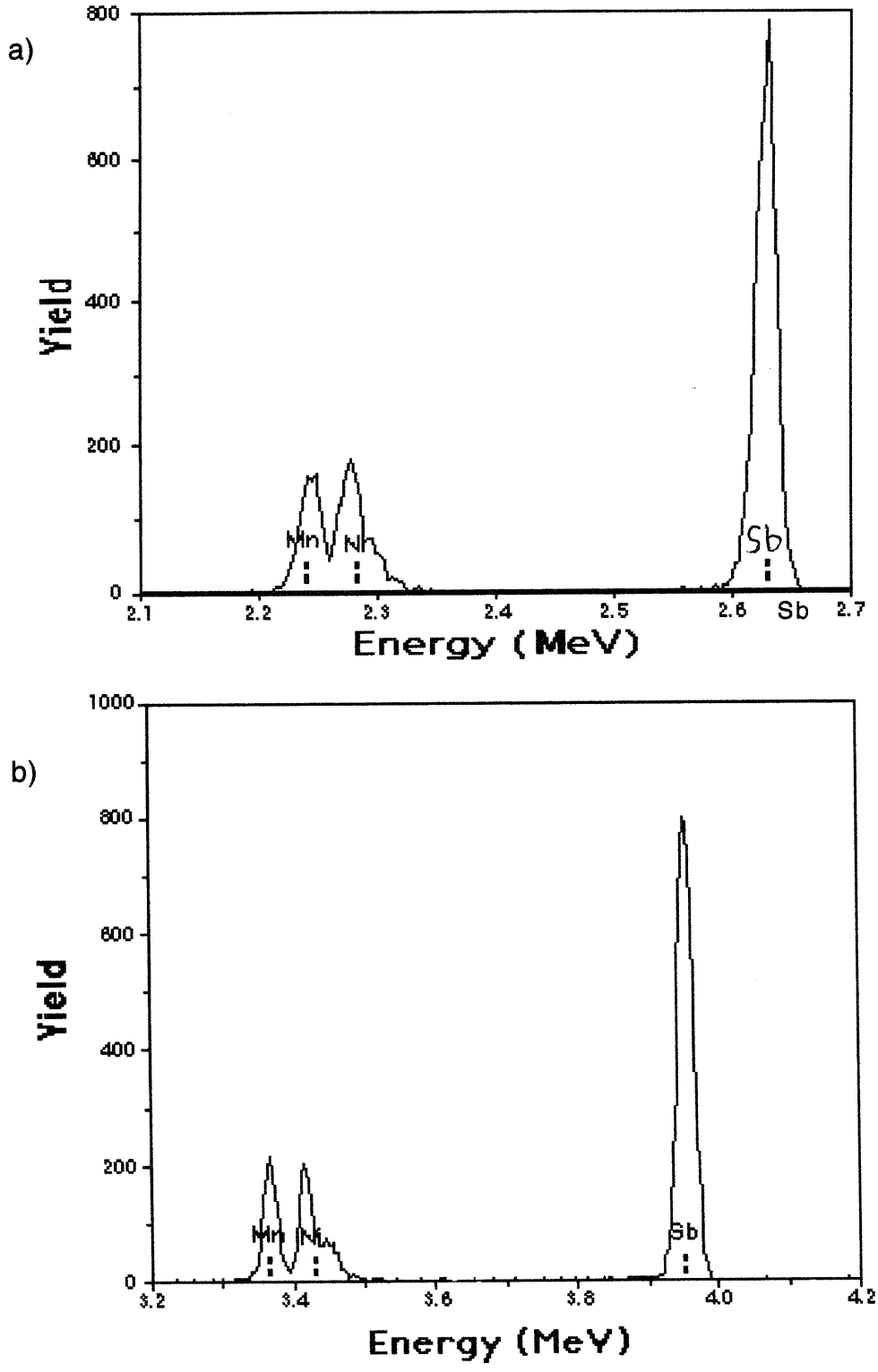

Figure 4.6: RBS spectra for 150 Å NiMnSb on Si
a) Sample 3 at 3.0 MeV b) Sample 3 at 4.5 MeV

4-4. Resistivity vs. Temperature

A sample of NiMnSb 1000 Å thick was prepared for four-terminal resistivity measurements. The resistance was measured with an AC resistance bridge, and the temperature with a silicon diode temperature sensor. The measurement was performed down to 4.2K. The plot of resistivity vs. temperature from 300K to 4.2K is shown in Figure 4.7a. Above about 70K, the resistivity increases linearly with temperature, which is consistent with the normal behavior for metals - in this temperature regime, phonon scattering due to lattice vibrations dominates over the scattering due to magnons. At very low temperatures, the influence of magnons becomes significant in normal ferromagnets as the thermally induced phonons are frozen out. Figure 4.7b shows the resistivity from 4.2 to 20K. The resistivity fits a quadratic equation over this range very well. However, the linear coefficient of the fit is a factor of five larger than the T^2 coefficient. In normal ferromagnets, the T^2 dependence of resistivity is the dominant effect, which results from the contribution of magnon scattering to the resistivity.[14] In addition from 4.2K to 11K the data does appear to show linear dependence as seen by Moodera and Mootoo.[13] Despite this, the absence of T^2 dependence is not entirely clear, and it is impossible to conclusively say whether the data is consistent or inconsistent with HMF.

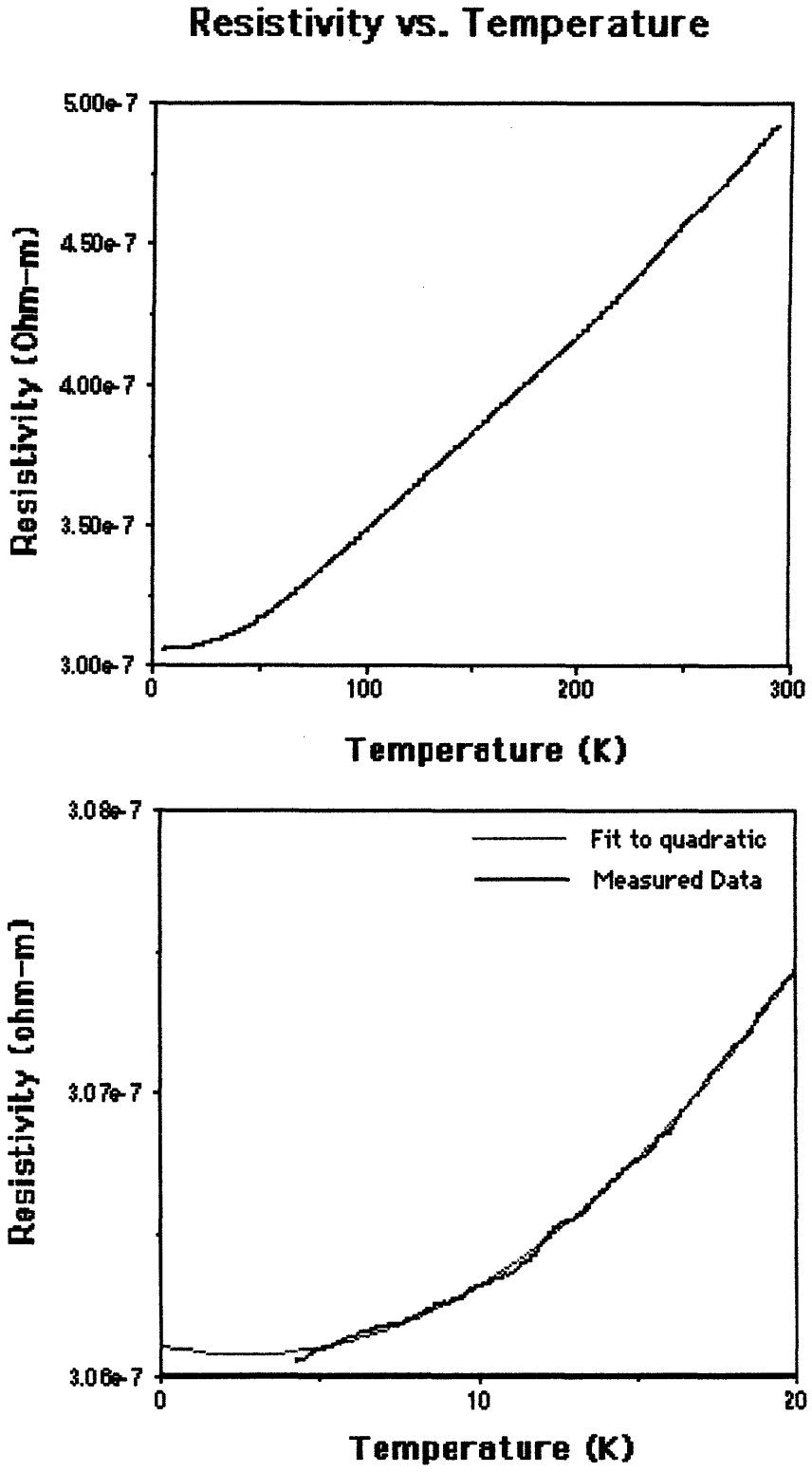

Figure 4.7 Resistivity Measurements a) 4.2K to 300K b)4.2K to 20K along with quadratic fit: $\rho=3.061X10^{-7} - 2.385X10^{-11} T + 4.538X10^{-12} T^2$.

5. Ferromagnet-Insulator-Ferromagnet Tunneling Experiment

5-1. Preparation of NiMnSb tunnel junctions

5-1.1 NiMnSb Deposition

The first step in the process (see Figure 5.1 for an illustration of junction preparation) is to deposit a broad strip of NiMnSb. The width of this strip eliminated problems of nonstoichiometry in the junction area due to shadowing from the edges of the mask used. The substrate temperature was varied from 300°C-500°C with most trials at 450°C, and the pressure during deposition was usually 3-5X10^{-7} torr. The thickness of the NiMnSb for most trials was 300 Å, although a few trials were performed with only 150 Å. After the NiMnSb deposition, the substrate was cooled rapidly with liquid nitrogen (LN_2) with the total cooling time from 450°C to ~77K being approximately 10 minutes. The copper block was held at this temperature for about 15 minutes to give the glass substrate sufficient time to cool completely.

5-1.2 Barrier Preparation

After the glass substrate was cooled to near 77 K, a thin layer of Al (14-29 Å) was deposited on top of the NiMnSb. The deposition was performed at low temperature in order to insure a smooth uniform layer of Al by limiting the mobility of the Al atoms during deposition and hence inhibiting growth by islanding. This layer of Al was then oxidized by glow discharge in an O_2 atmosphere of 75-100 mTorr to form the insulating tunnel barrier. The configuration of the glow discharge is shown in Fig 5.2. The upper Al plate was held at a high negative voltage of 450-550 volts, with either the substrate or the

Figure 5.1 Tunnel Junction Preparation

1) 300 Å NiMnSb at 450°C

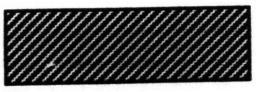

2) 14-29Å Al at 77K

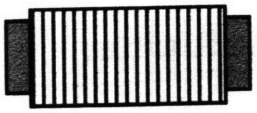

3) Glow Discharge at 300K

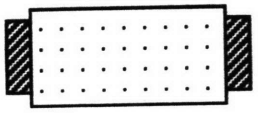

4) 120Å at 77K

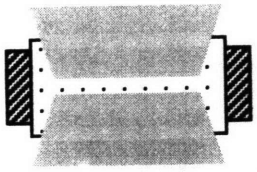

5) 200-300Å FM cross strips

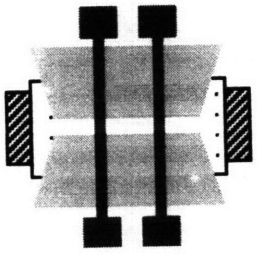

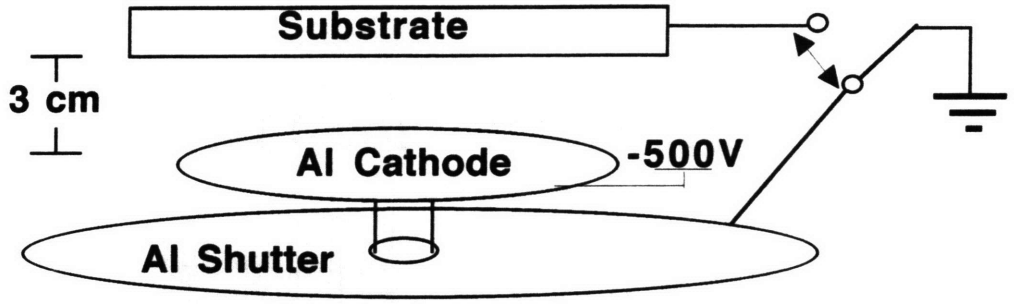

Figure 5.2 Configuration of Glow discharge.

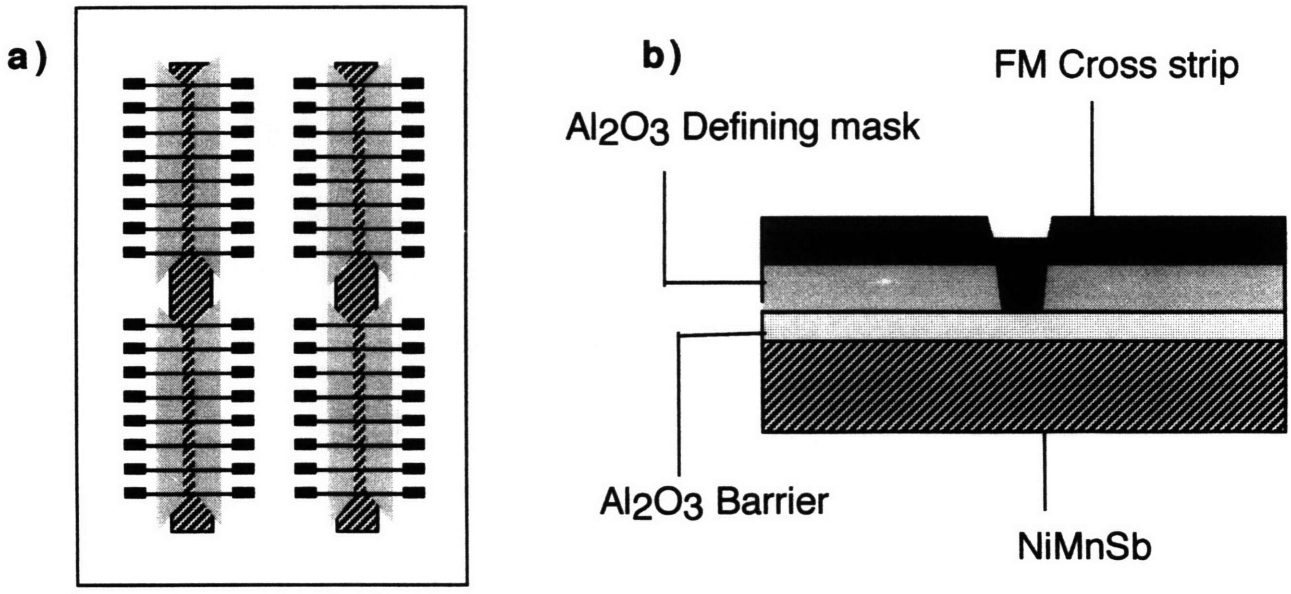

Figure 5.3 a) Completed set of junctions
b) Cross section of tunnel junction

lower plate held positive. The time of the glow discharge was varied from 30 seconds to up to six minutes. The barrier preparation is the key step in the process of producing good tunnel junctions. As mentioned earlier, tunneling is an extremely surface sensitive phenomenon, so these two steps must be performed in such a way that the NiMnSb surface integrity is maintained. If the Al layer is too thin, the glow discharge will oxidize past the Al layer and begin oxidizing the NiMnSb surface. If the Al layer is too thick or the glow discharge too short, a layer of Al will be left behind that could dramatically reduce the polarization observed since the tunneling electrons would essentially come from Al and not NiMnSb. In addition, the thickness of the oxide must be constrained to produce junctions with resistances of about 1KΩ-100 KΩ. Junctions with resistances above this range are generally more noisy and difficult to measure, while those with resistances significantly below this range have a greater likelihood of shorted low resistance pathways through the barrier that obscure the tunneling phenomenon.

5-1.3 Al_2O_3 Defining Mask

The NiMnSb strip as prepared was too broad to form useful junctions because of the large probability of shorting between the upper and lower electrodes in such a large area junction. Consequently, an Al_2O_3 defining area was deposited which narrowed the junction area to 0.7 mm. In order to perform this, the system had to be opened, and the Ni removed from the e^- beam crucible to be replaced with Al_2O_3 pellets. The crucible was thoroughly cleaned before being loaded with the Al_2O_3, and the system was subsequently pumped down for a few hours. After the system reached the high 10^{-8} torr range, 120 Å of Al_2O_3 was deposited from the e^- beam crucible through the defining mask to

insulate completely the NiMnSb strip from the upper electrode except in the junction area.

5-1.4 Ferromagnetic cross strips

Deposition of the top layer consisting of cross strips of ferromagnetic material completed the preparation of one set of tunnel junctions, consisting of a total of 32 individual junctions. A number of ferromagnets were tried as the upper electrodes, including NiFe (80% Ni), Co, and CoFe (~70% Fe). Most junctions were prepared with NiFe because its low coercivity usually placed it far from that of NiMnSb. Figure 5.3 shows a completed set of tunnel junctions along with a cross sectional view of a FM-I-FM tunnel junction.

5-2. FM-I-FM Tunneling results

5-2.1 Measurement of Tunnel Junctions

A four terminal measurement was performed on the junctions prepared as shown in Figure 5.4. The magnetic field was applied in the plane of the junctions and varied from +5 kGauss to -5 kGauss and back. The resistance was measured with a Linear Research LR700 AC resistance bridge and the field with a sensor near the poles of the electromagnet. The output from these instruments were fed into a computer equipped with a data acquisition card.

5-2.2 Tunneling Results

Many sets of junctions were prepared and analyzed, but only one series, 10-283, showed significant junction magnetoresistance (JMR) at room temperature. Figure 5.5 shows the JMR from one of these junctions at RT along with the magnetoresistance (MR) of the two electrodes. The arrows indicate the

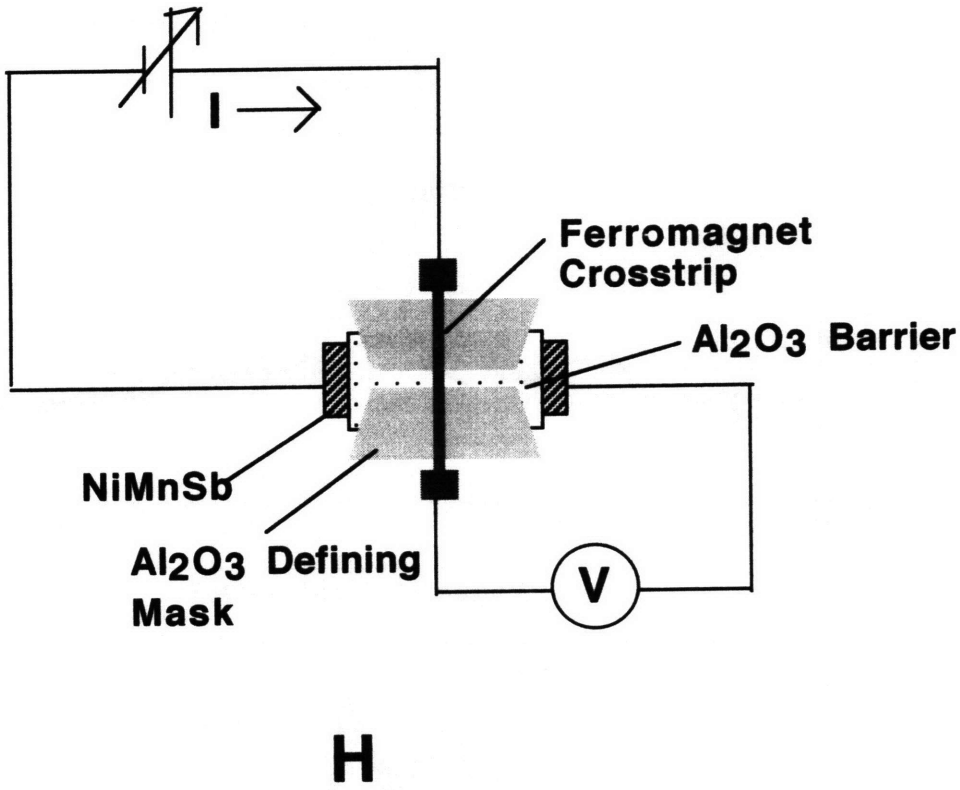

Figure 5.4 Measurement of Junction Magnetoresistance. The magnetic field is applied in the plane of the film.

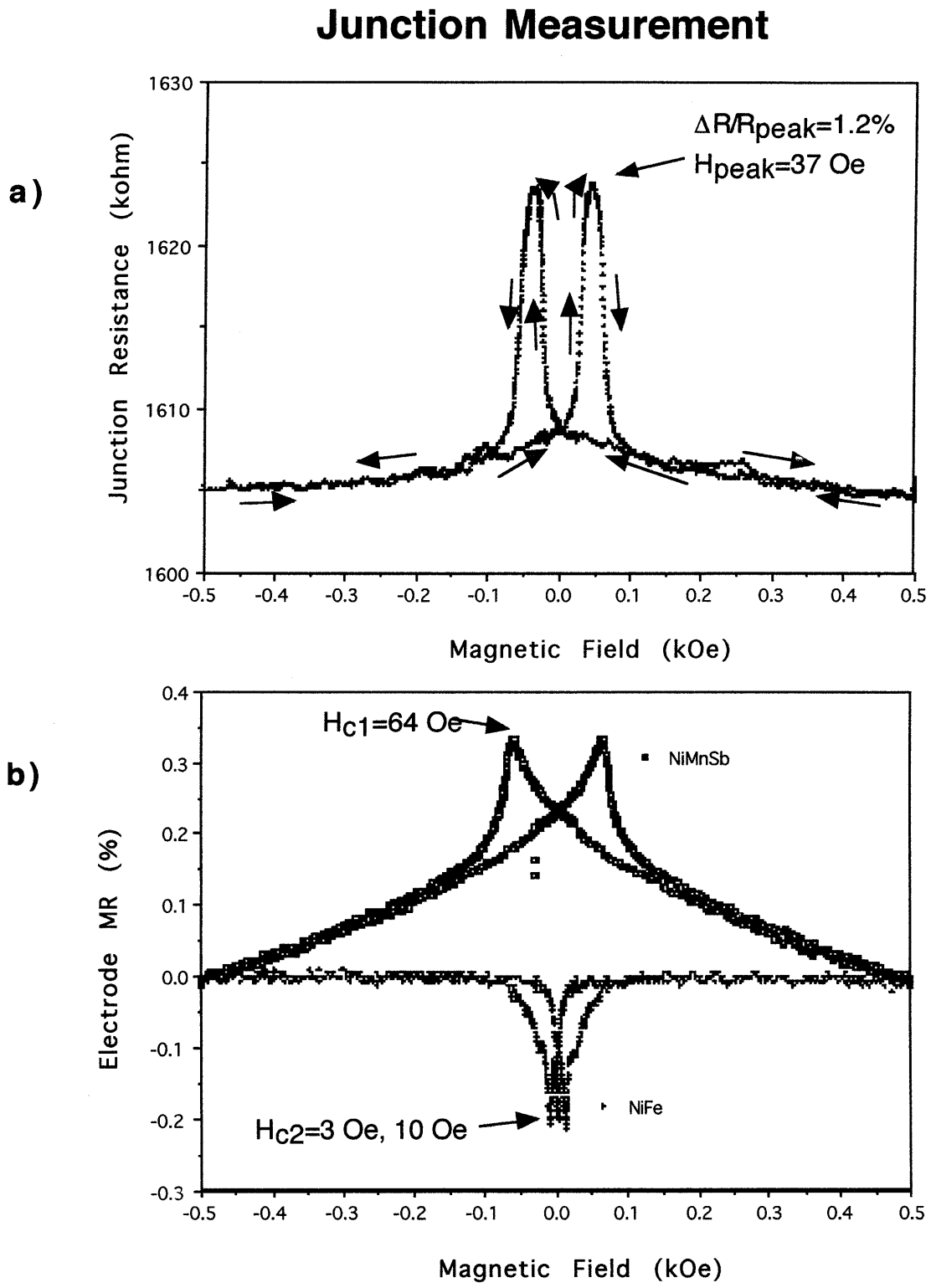

Figure 5.5 Measurement of NiMnSb/Al_2O_3/NiFe Junction at 300K
a) Junction Magnetoresistance b) Magnetoresistance of FM electrodes

progression of the magnetic field. Starting at high negative fields, the two electrodes are aligned parallel to each other, and the resistance is low. The resistance rises slowly as the field is reduced to zero. After the field is reversed, the resistance rises rapidly as the magnetically softer NiFe (80% Ni, 20% Fe) electrode reverses its magnetization. The resistance peaks at H=37 Oe with a maximum JMR of 1.2% measured with respect to the peak, and subsequently falls rapidly as the NiMnSb electrode aligns with the NiFe electrode. This explanation of the JMR behavior is confirmed by analyzing the MR of the electrodes. Since the current flow is perpendicular to the applied magnetic field in the NiMnSb electrode, it shows a peak in resistance, whose position roughly corresponds to the coercivity of the NiMnSb electrode. In this case the peak occurred at H=64 Oe. The current flow in the NiFe electrode is parallel to the field, and the NiFe shows a valley in resistance near its coercivity. The NiFe in fact shows two valleys at H=3 Oe and 10 Oe, which is probably due to the fact that different parts of the cross strip have different coercivites. Part of the cross strip lies on glass, while the other lies on Al_2O_3, and because the underlying layer can affect the coercivity strongly, the different parts of the NiFe strip could have different coercivities. In addition, the region in the junction area can also have a different coercivity because of magnetic coupling with the NiMnSb layer. Nevertheless, the coercivity of NiFe is clearly much lower than that of NiMnSb. Thus, as expected, the peak in JMR resides in the field region between the coercive fields of the two electrodes. Many other junctions from the 10-283 series showed similar behavior. The JMR at room temperature ranged from 1.0-1.5% for tunnel junctions from this series with resistances greater than 1 kΩ, while JMR was much smaller for junctions with smaller resistances. Possible microscopic shorts through the barrier in these latter junctions can account for

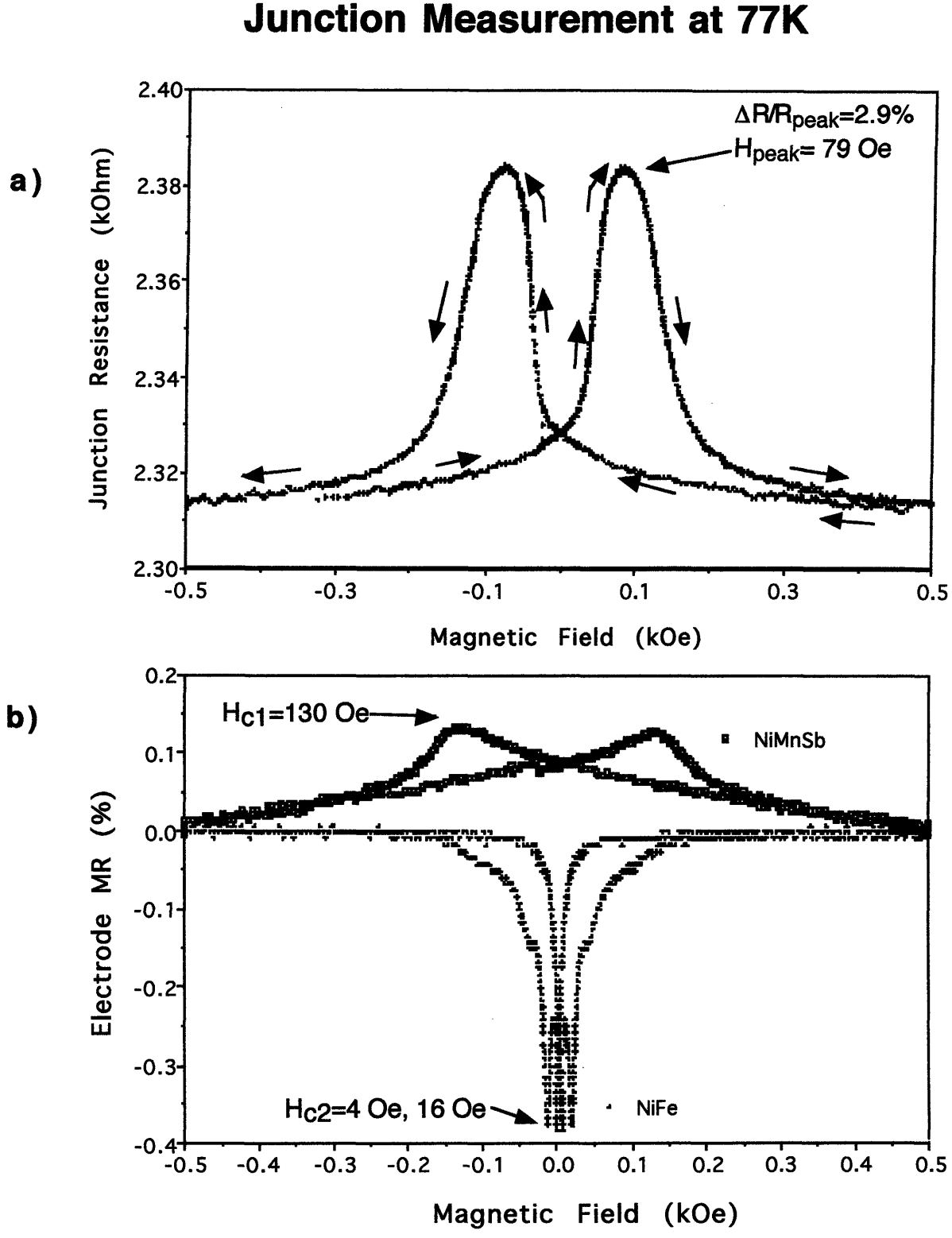

Figure 5.6 Measurement for NiMnSb/Al_2O_3/NiFe Tunnel Junction at 77K
a) Junction Magnetoresistance b) Magnetoresistance of FM electrodes

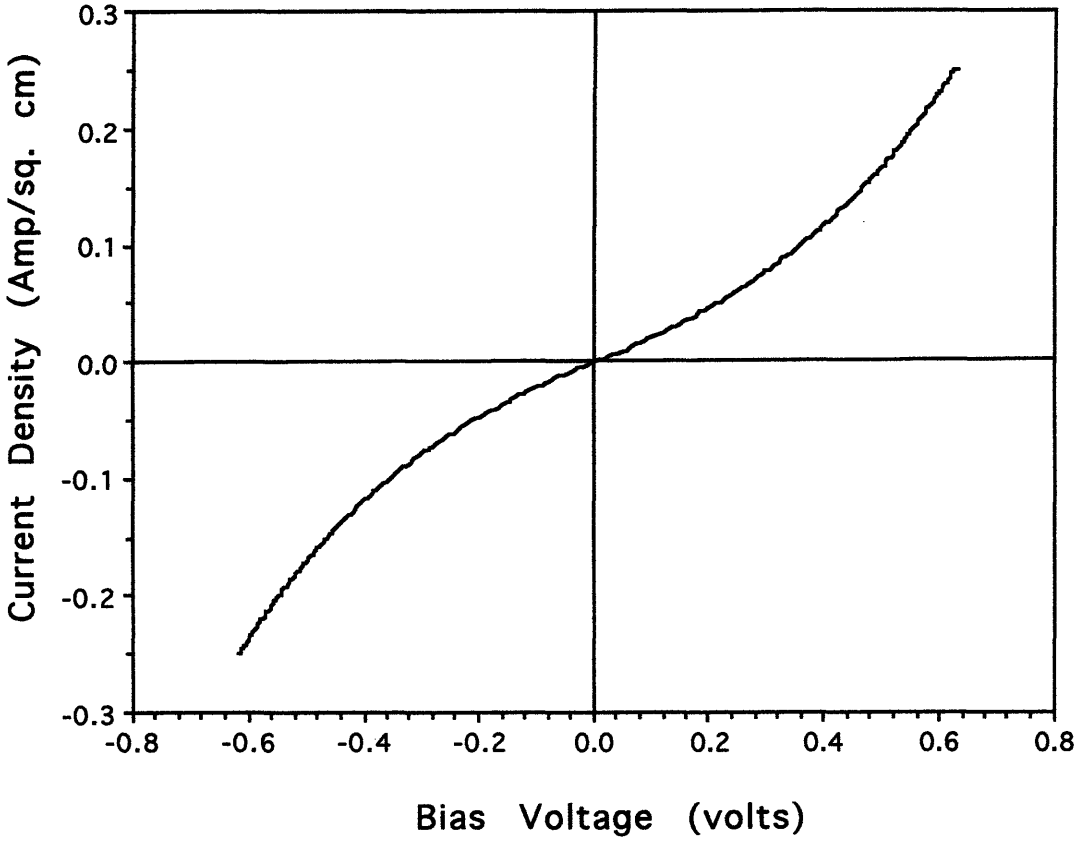

Figure 5.7 I-V characteristic for 10-283 NiMnSb/Al_2O_3/NiFe junction. Fit to Simmon's theory of tunneling gives a barrier height of 1.8 eV and a width of 17 Å.

the lower resistance and obscure the effect of any tunneling electrons.

The measurement for this series of junctions was repeated at 77K. The JMR of the junction in Figure 5.5 more than doubled to 2.9% as shown in Figure 5.6. Other junctions in this series showed a JMR of up to 4.5%. The increased JMR could be due to a number of factors. The MR of the electrodes indicates that the difference in the coercivities of the electrodes increased dramatically because of the large increase in the NiMnSb coercivity to 130 Oe. This results in a more strongly antiparallel orientation and, thus, a higher JMR. In addition, the detrimental effect of any magnetic oxides at the FM-I interfaces, which may result in spin scattering by paramagnetic ions, could be reduced due to antiferromagnetic ordering of these oxides below room temperature. Also, if NiMnSb is half-metallic, an increase in polarization with decreasing temperature is expected as the thermal excitations of minority spin electrons across the band gap is reduced.

Measurements of the current-voltage (I-V) characteristics of these junctions were performed in order to confirm that tunneling is indeed the mode of conduction between the FM electrodes. Figure 5.7 shows the I-V characteristic for one of the 10-283 junctions with > 1kΩ resistance. The current increases in a distinctly nonlinear manner at high bias voltages, which is characteristic of the tunneling phenomenon. The curve was fit to Simmon's theory of tunneling, which gave a barrier height (ϕ) of 1.8 eV and a barrier thickness (d) of 17 Å. These parameters are consistent with good Al_2O_3 tunnel barriers (ϕ~1.5-3.0eV) and the expected thickness of oxidized Al as measured by the quartz crystal monitors.

Many other junctions were prepared and measured, but the 10-283 series showed by far the best results. No other set showed significant JMR at

room temperature, although some did show 1-4% at 77K.

5-3. Discussion

The JMR observed even in the best cases was significantly lower than predicted by Julliere's model of FM-I-FM tunneling. Solving for the polarization of NiMnSb using Equation (1) using $\Delta R/R_{\uparrow\downarrow} = 4.5\%$ and $P_{NiFe}=28\%$ gives a polarization of 8.2% for NiMnSb. There are a number of possible reasons for this reduced JMR and observed spin polarization. As mentioned earlier, FM-I-FM tunneling is an extremely surface sensitive phenomenon. Consequently, the constraints for preparing good tunnel junctions are very stringent. Because the NiMnSb must be prepared at high temperatures, the probability of surface degradation of the NiMnSb is significant. This was the main reason that the annealing step was avoided, i.e. to minimize the time that the NiMnSb surface was exposed to high temperature. One possible problem is the segregation of one or two of the three component elements at the surface. This would change the composition at the surface of the NiMnSb, and consequently, the tunneling electrons will not be coming from 1:1:1 stoichiometric NiMnSb. Another potential problem at elevated temperatures is the rapid oxidation of the surface. XPS studies performed at New York University by Professor B. Sinkovic on one NiMnSb film indicates that oxidation of Mn is a major problem. A sputter cleaned surface left overnight at 10^{-10} Torr formed a monolayer or so of MnO on the NiMnSb surface. At elevated temperatures and worse vacuum conditions, this oxidation can occur much more readily. Either of these surface degrading properties can dramatically reduce the spin polarization of electrons coming from the NiMnSb electrode.

One serious problem encountered is the fact that the Al_2O_3 barriers prepared seemed to be of rather low quality in many cases. The quality of the barrier is critical to observe any spin dependent tunneling. Spin must be conserved in the tunneling process or any information on the spin polarization of the FMs is lost. Unfortunately, the junctions in many instances exhibited high signal noise during the junction measurement that made the measurement of the JMR difficult. This noise is probably due to the presence of trapped states within the barrier, which could arise due to the nature of the glow discharge. The high energy of ions involved in the glow discharge could damage the surface of the Al layer and lead to highly defected oxide layer. In addition, sputtering off of the cathode could result in some contamination of the barrier. The surface roughness of NiMnSb may also affect the quality of the Al_2O_3 barrier. A rough surface would result in shadowing effects that would make depositing a thin uniform layer of Al very difficult. Examination of the x-ray patterns did seem to indicate a correlation between surface roughness and the quality of the tunnel junction. Series 10-285, 10-286 and 10-288 (see Figures 4.3a-b and 4.4) all showed strong preferential growth in the (111) direction which results in a rough pyramid-like structure. These sets all showed zero JMR. In contrast, series 10-283 and 10-284 showed a more subdued (111) peak and less preferential growth in this direction. These two sets also showed better than average JMR results - 10-283 showing up to 1.5% at RT and 4.5% at 77K, while 10-284 showed up to 4.5% at 77K (although JMR was flat at RT). It should be noted that 10-283 and 10-286 were prepared with virtually identical deposition parameters, yet 10-286 shows a much more prominent (111) peak. This suggests that the growth of NiMnSb, especially the crystallite orientation, needs to be better controlled and understood.

6. Conclusions

FM-I-FM tunnel junctions were prepared with NiMnSb as one electrode. X-ray diffraction and Rutherford back scattering measurements indicated that the $C1_b$ NiMnSb compound was being formed with the desired ratio 1: 1: 1 within experimental error. These tunnel junctions showed a JMR of only up to 1.5% at room temperature and 4.5% at 77K. These results are an order of magnitude lower than the value expected from Julliere's model, and deGroot's prediction of half-metallic ferromagnetism remains unconfirmed experimentally. The primary problem encountered that may have degraded the JMR was the difficulty in forming a good tunneling barrier. In many cases the junctions showed a very noisy signal which indicates that the barrier quality was poor. Surface degradation of the NiMnSb may also have diminished the observed JMR.

One problem that could contribute to the difficulty in preparing good tunnel junctions is the surface roughness of the NiMnSb. The x-ray diffraction patterns indicate that there is some correlation between the quality of the junction and the preferred orientation of the NiMnSb- those junctions prepared on NiMnSb showing no preference in the (111) orientation gave the best results. This indicates that better control of the NiMnSb growth is needed to suppress the (111) orientation, which results in a rougher, pyramid-like structure. This may be achieved by using a substrate other than glass and approaching epitaxial growth by depositing at much lower rates. However, contamination by residual gases becomes a greater problem with low deposition rates, and a much better vacuum would be required.

The nature of the glow discharge may also diminish the quality of the

insulating barrier, either by damaging the Al layer during oxidation or by sputtering of impurities off the cathode onto the substrate. The former can be prevented by either shielding the substrate from a direct view of the cathode or by decreasing the voltage applied to the cathode to decrease the energy of the ions during the glow discharge. However, control of the voltage is rather limited because a minimum voltage is needed for a self-sustained glow discharge. Addition of a small filament source of electrons can compensate for this and result in a higher density of ions. Performing the glow discharge in an area well shielded from the evaporation sources would also be beneficial by eliminating the possibility of impurity sputtering from the cathode. In situ surface characterization techniques would be extremely useful in determining the surface quality of the NiMnSb before and after the formation of the tunneling barrier.

References.

1. R.A. deGroot, F.M. Mueller, P.G. van Engen, and K.H.J. Buschow, **Phys. Rev. Lett.** 50, 2024 (1983).

2. R. Meservey, P. M. Tedrow, **Phys. Rev. B** 7, 318 (1973).

3. R. Meservey, P.M. Tedrow, **Physics Reports (Review Section of Physics Letters)** 238, No. 4 (1994) 173-243.

4. J.S. Moodera, Lisa R. Kinder, Terrilyn M. Wong, and R. Meservey, **Phys. Rev. Lett.** 74, 3273-6. (1995)

5. M. Julliere, **Phys. Lett.** 54A, 225 (1975).

6. Watanabe, **Trans. Jpn Inst. Met.** 17, 220 (1976).

7. E. Persson, **Naturwiss.** 16, 613 (1928).

8. E. Persson, **Z. Physik.** 57, 115 (1929).

9. A.J. Bradley and J.W. Rodgers, **Proc. Royal Soc. A** 144, 340 (1934).

10. A.R. Williams, J. Kubler, and C.D. Gelatt Jr., **Phys. Rev.** B19, 6094 (1979).

11. M. Methfessel and J. Kubler, **J. Phys. F** 12, 141 (1982).

12. Kabani, R.N., Ph.D. Thesis, Tufts U. (1992).

13. J.S. Moodera and D.M. Mootoo, **J. Appl. Phys.**, 76, 6101-3.

14. G.K. White and S.B. Woods, **Philos. Trans. R. Soc. London A** 251, 273 (1958).

15. G.L. Bona, F. Meier, M. Taborelli, E. Butcher and P.H. Schmidt, **Solid State Comm.** 56(4), 391 (1985).

16. C. Rau and A.R. Koymen, **SPIE** 836, 9933 (1987).

17. M.M. Kirillova, A.A. Makhnev, E.I. Shreder, V.P. Dyakina and N.B. Gorina, **Phys. Stat. Sol. (b)** 187, 231 (1995).

18. T. Miyazaki and N. Tezuka, **J. Magn. Magn. Mater.** 126 (1995) L231.

19. L. Castelliz, **Monatsh. Chem.** 83, 1314 (1952).